Journal of Science and Transport Technology
Journal homepage: https://jstt.vn/index.php/en

Dynamic Response of a Viscoelastic FG Beam under Axial Compression and Moving Harmonic Loads

Tran Van Lien[1], Le Thi Ha[2*]
[1]Department of Building and Industrial Construction, Hanoi University of Civil Engineering, Hanoi, Vietnam
[2]Department of Basic Sciences, University of Transport and Communications, Hanoi, Vietnam

Article info
Type of article:
Original research paper

DOI:
https://doi.org/10.58845/jstt.utt.2026.en.6.4.62-75

[*]**Corresponding author:**
Email address:
lethiha@utc.edu.vn

Received: 02/12/2025
Received in Revised Form: 18/05/2026
Accepted: 09/06/2026

Abstract: This study investigates dynamic response of a viscoelastic FG beam under axial compression and moving harmonic loads. The Mori–Tanaka model is used to determine the thickness-wise power-law material properties of the beam. The Kelvin–Voigt model is used to represent viscoelastic damping in the beam. General motion equations are established using FEM. A parametric study is performed to investigate the effects of material distribution, damping, convoy velocity, axial compressive force, inter - load spacing, and excitation frequency on the dynamic response. Numerical simulations demonstrate that these parameters have a pronounced effect on the dynamic deflection response of FG beams.

Keywords: FGM, damping, Timoshenko beam, moving harmonic load, axial compressive force.

1. Introduction

The problem of beams under moving forces has been widely studied since the 19th century, following a bridge collapse in England that first highlighted the importance of this phenomenon. Henchi et al. [1] showed that the Wittrick–Williams algorithm yields exact natural frequencies and mode shapes for multi-span beams under moving harmonic loads. Kim [2] analyzed beams under axial compression and moving loads with constant or harmonic amplitude. In this study, a uniformly distributed load moving at constant speed and a linear hysteretic damping foundation are considered. Kocatürk [3] used Lagrange's equations to analyze axially loaded beams under eccentric compression and a moving harmonic point load. Furthermore, Cai [4] employing Fourier and Laplace transformations, calculated the response of modified Timoshenko thin-walled beams in bending and torsional vibration subjected to moving harmonic loads.

Recently, significant research interest has been directed toward the dynamic analysis of FG beams subjected to moving forces. The beam's dynamic response is evaluated with respect to material distribution, load velocity, and excitation frequency. Şimşek et al. [5, 6] studied the free vibration and dynamic response of a simply supported FG beam under a harmonically varying moving point load using the Euler-Bernoulli beam model. Şimşek [7] used the Timoshenko beam theory (TBT) to study nonlinear dynamic responses of a pinned–pinned FG beam under a moving harmonic force. Employing both Euler–Bernoulli and TBT, Wang [8], examined the forced vibrations of an axially FG beam subjected to moving force in a thermal environment. The effective material properties of the FG beam are evaluated using the Voigt model and the Mori-Tanaka homogenization model. Using the TBT, in [9], Şimşek studied the vibration behavior of sandwich FG beams subjected to two harmonic moving forces with constant speeds. Using the Ritz method in conjunction with Newmark's time-integration scheme, Songsuwan [10] analyzed the vibration behavior of sandwich FG beams supported by a Pasternak foundation under harmonic loading.

Considering damping effects, Akbas [11] examined the vibration behavior of viscoelastic microbeams subjected to external excitation by applying the size-dependent theory together with the Kelvin-Voigt viscoelastic model. Ding et al. [12] examined the effect of damping ratios on the natural frequencies associated with transverse vibrations in axially moving viscoelastic beams, employing the Euler-Bernoulli beam theory in conjunction with the Kelvin-Voigt model. Mohseni and Shakouri [13] studied the free vibration, damping, and forced response of sandwich plates with a viscoelastic core and graphene-reinforced face sheets. Akbas et al. [14] conducted a dynamic investigation of composite deep beams containing FG porosity subjected to sine pulse loads. In [15], Yee et al. analyzed the coupled dynamics of viscoelastic shear-deformable beams reinforced with graphene nanoplatelets, featuring axial functional grading and incorporating both geometrical and material imperfections. Cui et al. [16] examined the vibration behavior of viscoelastic FG beams using the Kelvin–Voigt fractional-order model and quasi three dimensional beam theory.

The Kelvin-Voigt model has simple mathema-tical structure. It accurately models materials that recover all of their deformation over time after a load is removed and provides reasonable behavior for viscoelastic materials at low frequencies. However, the Kelvin-Voigt model is limited by its inability to accurately describe stress relaxation and its failure to model permanent deformation because the dashpot is constrained by the spring. It is best suited for modeling creeping solids. The model behaves non-physically at high frequencies. To overcome these limitations, complex models like the Standard Linear Solid or fractional Kelvin-Voigt models are used. For most practical purposes, the Kelvin – Voigt model is adequate [17].

Existing investigations into damping effects on beam dynamics are limited, and commonly adopt a prescribed constant damping ratio. Previous studies have not considered prescribed ranges of damping ratios or evaluated how changes in these ratios affect structural dynamic responses. Recently, Lien and Ha determined the ranges of damping ratios on the forced vibration of the microbeams [18] and macrobeams [19] under a constant moving force.

A comprehensive investigation of the vibration characteristics of viscoelastic FG beams under axial compression and a convoy of moving harmonic loads is still lacking in the literature. In this study, the forced vibration response of an FG beam under axial compression and a convoy of moving harmonic loads is analyzed based on the TBT combined with the Kelvin-Voigt viscoelastic model. The time-domain solution is obtained using the finite element method in conjunction with Newmark's implicit integration procedure. The study investigates how material properties, damping ratios, load velocities, load spacing, excitation frequency, and axial compression affect the forced vibration of the FG beam.

2. Basic relations

Fig. 1 shows the FG beam with length L, width b, height h and a rectangular cross section. The beam is subjected to an axial compressive force and multiple equally spaced point loads with spacing d. The point loads move across the beam at constant speed and remain continuously applied to the beam. The volume fraction of material changes through the height as given below:

$$V_c(z) = (0.5 + z/h)^n ; -0.5 \le z/h \le 0.5 \quad (1)$$

In Eq. (1), n denotes a material parameter, and z indicates the distance from the mid-plane of the beam; Here, c is a subscript indicating ceramic materials. The effective bulk and shear moduli, K_f and G_f, are obtained using the Mori–Tanaka model as:

$$K_f(z) = K_{fm} + \frac{(K_{fc} - K_{fm})V_c(z)}{1 + (1 - V_c(z))(K_{fc} - K_{fm})/(K_{fm} + 4G_{fm}/3)};$$
$$G_f(z) = G_{fm} + \frac{(G_{fc} - G_{fm})V_c(z)}{1 + \dfrac{(1 - V_c(z))(G_{fc} - G_{fm})}{G_{fm} + G_{fm}(9K_{fm} + 8G_{fm})/(6K_{fm} + 12G_{fm})}} \tag{2}$$

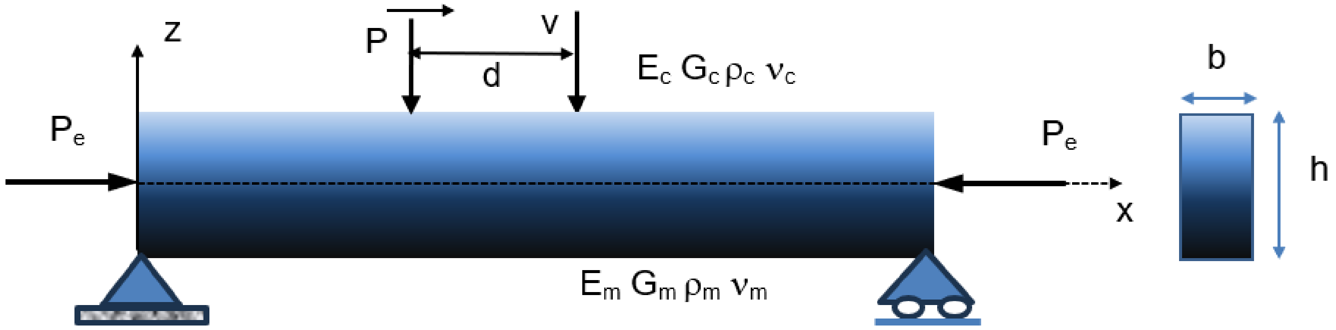

Fig. 1. A FG beam under the axial compression force and multiple moving loads

The FG material beam's effective material properties, including Young's modulus E_f, Poisson's ratio ν_f, and the mass density ρ_f may be calculated as given below:

$$E_f(z) = \frac{9K_f(z)G_f(z)}{3K_f(z) + G_f(z)};$$
$$\nu_f(z) = \frac{3K_f(z) - 2G_f(z)}{2[3K_f(z) + G_f(z)]}; \tag{3}$$
$$\rho_f(z) = \rho_{fc}V_c(z) + \rho_{fm}[1 - V_c(z)];$$

According to the TBT, the displacement field of the FGM beam is given by:

$$u_b(x_b,z,t) = u_{b0}(x_b,t) - (z - h_0)\theta_b(x_b,t);$$
$$w_b(x_b,z,t) = w_{b0}(x_b,t); \tag{4}$$

In Eq. (4) $u_{b0}(x_b,t), w_{b0}(x_b,t)$ represent the axial and transverse displacements of any point along the neutral axis; θ_b is the cross-sectional rotation, while h_0 denotes the distance between the neutral axis and the x-axis, defined by the zero axial force condition:

$$h_0 = \frac{\int_A zE_f(z)dA}{\int_A E_f(z)dA} \tag{5}$$

In the TBT, normal strain and shear strain are given by:

$$\varepsilon_{xx} = u_{b0,x}(x_b,t) - (z - h_0)\theta_{b,x}(x_b,t);$$
$$\gamma_{xz} = w_{b0,x}(x_b,t) - \theta_b(x_b,t); \tag{6}$$

Using the Kelvin-Voigt damping model, the constitutive relations for the functionally graded material beam are given by [14-16]

$$\sigma_{xx} = E_f\varepsilon_{xx}(x_b,t) + \eta_1\dot{\varepsilon}_{xx}(x_b,t)$$
$$= E_f(\varepsilon_{xx} + \varsigma_1\dot{\varepsilon}_{xx}) \text{ with: } \varsigma_1 = \frac{\eta_1(z)}{E_f(z)}$$
$$\sigma_{xz} = k_sG_f\varepsilon_{xz} + k_s\eta_2\dot{\varepsilon}_{xz} \tag{7}$$
$$= k_sG_f(\varepsilon_{xz} + \varsigma_2\dot{\varepsilon}_{xz}) \text{ with: } \varsigma_2 = \frac{\eta_2(z)}{G_f(z)}$$

where k_s is the shear correction coefficient, for a rectangular cross section k_s=5/6; ς_1, ς_2 denote the damping ratios for bending and shear, respectively.

Using expressions (4), (6), and (7), one gets the strain energy U_b [18]:

$$U_b = \frac{1}{2}\int_0^L \left[A_{11}u_{0,x}^2 - 2A_{12}u_{0,x}\theta_{,x} + A_{22}\theta_{,x}^2 + k_sA_{33}(w_{0,x} - \theta)^2\right]dx \tag{8}$$

the kinetic energy T_b:

$$T_b = \frac{1}{2}\int_0^L \left\{ I_{11}\left[\left(\dot{u}_0\right)^2 + \left(\dot{w}_0\right)^2 \right] - 2I_{12}\dot{u}_0\dot{\theta} + I_{22}\dot{\theta}^2 \right\} dx \quad (9)$$

and the dissipation function R_b:

$$R_b = \frac{1}{2}\int_0^L \left[C_{11}\left(\dot{u}_{0,x}\right)^2 - 2C_{12}\dot{u}_{0,x}\dot{\theta}_{,x} + C_{22}\left(\dot{\theta}_{,x}\right)^2 + k_s C_{33}\left(\dot{w}_{0,x} - \dot{\theta}\right)^2 \right] dx \quad (10)$$

Here A_{11}, A_{12}, A_{22}, A_{33} are the rigidities, respectively:

$$A_{11} = \int_A E_f(z)dA; A_{12} = \int_A E_f(z)(z-h_0)dA; \quad (11a)$$
$$A_{22} = \int_A E_f(z)(z-h_0)^2 dA; A_{33} = \int_A G_f(z)dA;$$

I_{11}, I_{12}, I_{22} are the mass moments, respectively:

$$I_{11} = \int_A \rho_f(z)dA; I_{12} = \int_A \rho_f(z)(z-h_0)dA \quad (11b)$$
$$I_{22} = \int_A \rho_f(z)(z-h_0)^2 dA;$$

and C_{11}, C_{12}, C_{22}, and C_{33} are the damping coefficients, respectively:

$$C_{11} = \int_A E_f(z)\varsigma_1(z)dA; C_{12} = \int_A E_f(z)\varsigma_1(z)(z-h_0)dA;$$
$$C_{22} = \int_A E_f(z)\varsigma_1(z)(z-h_0)^2 dA; C_{33} = \int_A G_f(z)\varsigma_2(z)dA; \quad (11c)$$

The strain energy due to the axial force P_e:

$$U_F = \frac{P_e}{2}\int_0^L \left(w_{,x}\right)^2 dx \quad (12)$$

The work of the external harmonic point load P_g can be written as follows:

$$V_b = \sum_{m=1}^{numload}\int_0^L P_g \cos(\Omega t) w_p\left(x_{pp}\right)\delta\left(x_{pp} - vt_m\right)dx \quad (13)$$

In Eq. (13), δ(.) denotes the Dirac-delta operator, x_{pp} denotes the present distance of force P_g from the beam's left end along the x-axis, w_{pp} denotes transverse displacement at the application point of the force P_g, and Ω is the excitation frequency.

3. Governing equation of an FGM beam

For the finite element formulation, the beam is divided into a sequence of two-node Timoshenko beam elements. Each node has three degrees of freedom: u, w and θ. The element displacement vector, denoted by $\mathbf{d_f}$, is expressed as:

$$d_f = \left\{u_{ii}, w_{ii}, \theta_{ii}, u_{jj}, w_{jj}, \theta_{jj}\right\}^T \quad (14)$$

In Eq. (14), the subscript ii refers to the left node; jj refers to right nodes; Accordingly, the axial displacement, the transerve displacement and the rotation of the cross section of the beam element are approximated by:

$$\begin{Bmatrix} u_{b0} \\ w_{b0} \\ \theta_b \end{Bmatrix} = \begin{bmatrix} N_u^1 & 0 & 0 & N_u^2 & 0 & 0 \\ 0 & N_w^1 & N_w^2 & 0 & N_w^3 & N_w^4 \\ 0 & N_\theta^1 & N_\theta^2 & 0 & N_\theta^3 & N_\theta^4 \end{bmatrix} \begin{pmatrix} u_{ii} \\ w_{ii} \\ \theta_{ii} \\ u_{jj} \\ w_{jj} \\ \theta_{jj} \end{pmatrix} = \begin{bmatrix} N_u \\ N_w \\ N_\theta \end{bmatrix} .d_f \quad (15)$$

In equation (15) N_u^1, N_u^2 denote Lagrange's shape functions; $N_w^i, N_\theta^i;\ i = \overline{1,4}$ denote Kosmatka's shape functions [20]. Using Eq. (15), the total strain energy srored in the beam in Eq. (8) is rewritten in matrix form as follows:

$$U_b = \frac{1}{2}\sum^{el} \mathbf{d}_f^T\left(\mathbf{k}_{11} + \mathbf{k}_{12} + \mathbf{k}_{22} + \mathbf{k}_{31}\right)\mathbf{d}_f \quad (16)$$

where el represents the number of elements employed in the discretization of the beam, and

$$\begin{aligned} \mathbf{k}_{11} &= \int_0^L N_{u,x}^T A_{11} N_{u,x} dx \\ \mathbf{k}_{12} &= -2\int_0^L N_{u,x}^T A_{12} N_{\theta,x} dx \\ \mathbf{k}_{22} &= \int_0^L N_{\theta,x}^T A_{22} N_{\theta,x} dx \\ \mathbf{k}_{31} &= k_s\int_0^L \left(N_{w,x} - N_\theta\right)^T A_{33}\left(N_{w,x} - N_\theta\right)dx \end{aligned} \quad (17)$$

From equation (9), the kinetic energy is rewritten in the following form:

$$T_b = \frac{1}{2}\sum^{el} \dot{\mathbf{d}}_f^T\left(\mathbf{m}_{11} + \mathbf{m}_{12} + \mathbf{m}_{22}\right)\dot{\mathbf{d}}_f \quad (18)$$

In Eq. (18)

$$m_{11} = \int_0^L N_{u,x}^T I_{11} N_{u,x} dx + \int_0^L N_{w,x}^T I_{11} N_{w,x} dx;$$
$$m_{12} = -2\int_0^L N_{u,x}^T I_{12} N_{\theta,x} dx; \quad (19)$$
$$m_{22} = \int_0^L N_{\theta,x}^T I_{22} N_{\theta,x} dx;$$

The dissipation function in Eq. (10) can be rewritten as follows:

$$R_b = \frac{1}{2}\sum^{el} \dot{\mathbf{d}}_f^T \left(\mathbf{c}_{11} + \mathbf{c}_{12} + \mathbf{c}_{22} + \mathbf{c}_{33}\right)\dot{\mathbf{d}}_f \quad (20)$$

where

$$c_{11} = \int_0^L N_{u,x}^T C_{11} N_{u,x} dx;$$
$$c_{12} = -2\int_0^L N_{u,x}^T C_{12} N_{\theta,x} dx$$
$$c_{22} = \int_0^L N_{\theta,x}^T C_{22} N_{\theta,x} dx \quad (21)$$
$$c_{33} = k_s \int_0^L \left(N_{w,x} - N_\theta\right)^T C_{33} \left(N_{w,x} - N_\theta\right) dx$$

The strain energy due to the axial force in Eq. (12) may be written in a matrix form as:

$$U_{P_e} = \frac{1}{2}\sum^{n_e} \mathbf{d}_f^T \mathbf{k}_{P_e}^e \mathbf{d}_f \quad (22)$$

where $\mathbf{k}_{P_e}^e$ is the geometric stiffness matrix:

$$\mathbf{k}_{P_e}^e = \int_0^L N_{w,x}^T P_e N_{w,x} dx; \quad (23)$$

The work in Eq. (13) is derived as:

$$V_b = \sum^{ne} \mathbf{d}_f^T f_e \quad (24)$$

Here f_e denotes the time-dependent nodal force vector, whose components are zero for all elements except the one on which the moving load is acting:

$$f_e = \sum_{i=1}^{nload} P_{gi} \cos(\Omega t)\left(N_w\right)^T\Big|_{x_P} \quad (25)$$

and x_p denotes the present distance of moving load P from the beam's left end along the x-axis.

Accordingly, the finite element discretization yields the following form of the equations of motion for the viscoelastic FG beam [21]:

$$-\frac{d}{dt}\left(\frac{\partial T_b}{\partial \dot{d}_j}\right) + \frac{\partial\left(T_b - U_b - U_{P_e} + V_b\right)}{\partial d_j} - \frac{\partial R_b}{\partial \dot{d}_j} = 0 \quad (26)$$

The Lagrange's equations of Eq. (26) can be obtained as follows:

$$M_f \ddot{D}_f(t) + C_f \dot{D}_f(t) + K_f D_f(t) = F(t) \quad (27)$$

Here $D_f, \dot{D}_f, \ddot{D}_f$ are the displacement, velocity, and acceleration vector, respectively; $\mathbf{K_f}$, $\mathbf{C_f}$, $\mathbf{M_f}$ are the stiffness, damping and mass matrices, respectively; **F** is the load vector in the global coordinate system. The Newmark implicit integration method with γ = 1/2 and β = 1/4 [21], which guarantees unconditional convergence, is employed here to solve Eq. (27).

4. Numerical investigation

For convenience of presentation, the mid-span normalized dynamic deflection $w_d(L/2,t)/w_{00}$ (ndd) and the dynamic magnification factor (dmf) f_D of the simply supported beam are defined as follows:

$$f_D = \max\left[\frac{w_d(L/2,t)}{w_{00}}\right];\ w_{00} = \frac{PL^3}{48E_m I};$$
$$I = \frac{bh^3}{12};\ P_g = P_0 \cos(\Omega t); \quad (28)$$

This section presents a numerical investigation of the dynamic response of a simply supported FG beam under an axial compressive force P_e and different moving harmonic loads. The FG beam made of steel with material parameters [5]: E_m=210GPa, ρ_m=7800kg/m^3; and alumina (Al_2O_3) with material parameters: E_c=390GPa, ρ_c=3960kg/m^3 is considered. The FG beam with length L, width b and height h are specified as follows [5]: h= 0,9m, b=0,4m and the ratio L/h=20. Furthermover, due to the scarcity of studies on viscoelastic beams, the damping ratio is selected as, therefore the damping ratios ς_1 and ς_2 are assumed to have the same value $\varsigma_1 = \varsigma_2 = \varsigma$, within the interval from 0 to 10^{-1} in this study.

Table 1. Check the convergence of the computational program (n=2, Ω=0, Pe=0, three loads, d=L/4).

No of el.	2	4	6	8	10	12	18	20	40
f_D	0.9309	2.1197	1.8728	1.8879	1.8879	1.8879	1.8879	1.8879	1.8879

Table 2. Changes of the dmf of the FGM beam under a moving force when Ω=0 and P_e=0.

n	f_D Present	v (m/s)	f_D Símsek [5]	v (m/s) [5]
0.2	1.0648	219	1.0344	222
0.5	1.1816	195	1.1444	198
1	1.2828	176	1.2503	179
2	1.3648	162	1.3376	164
Full alumina	0.9370	251	0.9328	252
Full metal	1.7402	131	1.7324	132

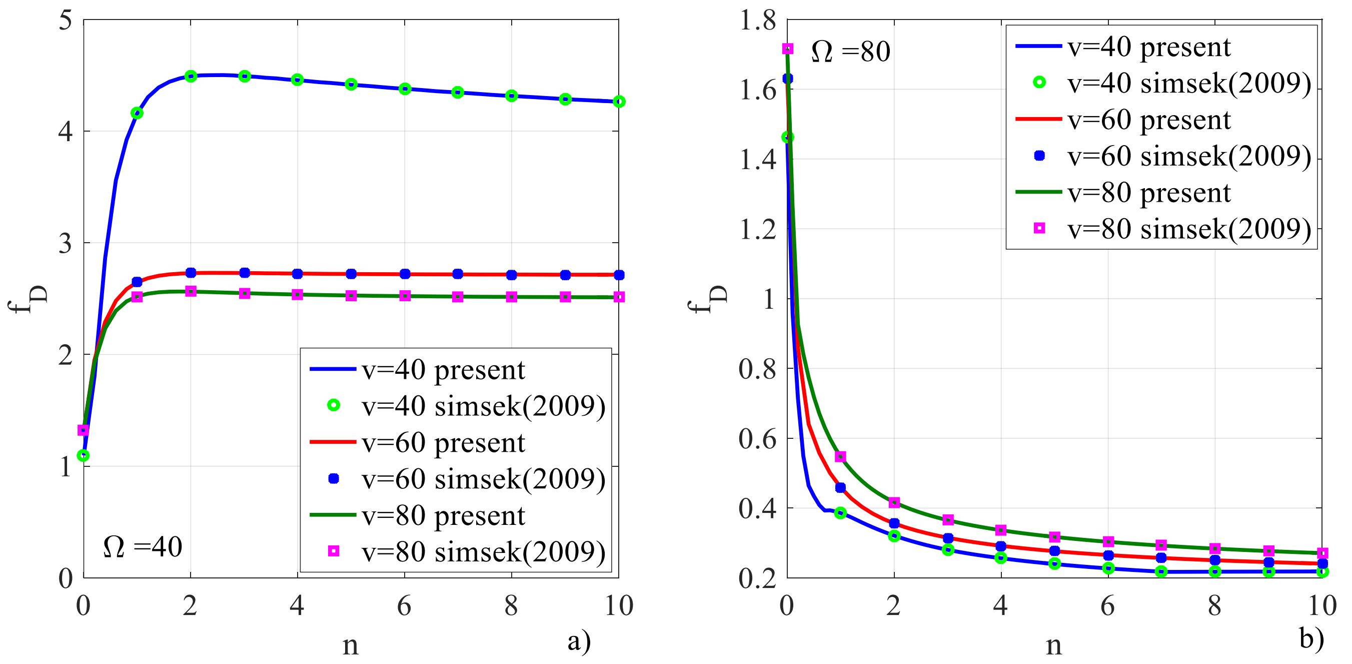

Fig. 2. Changes of the ndds at the mid-span with the various n when P_e =0: a) Ω=40rad/s, b) Ω=80rad/s.

A convergence study is performed first for the proposed finite element. Table 1 demonstrates the convergence of the developed finite element program. It can be observed that when the number of elements is 10, the dmf of the system shows good convergence. In the following calculations, the beam is divided into 40 elements, providing a sufficiently fine discretization for forced vibration analysis.

To assess the accuracy of the present FEM approach, numerical results are compared with those reported by Simsek and Kocatürk [5] in Table. 2 and Fig. 2, as well as with Henchi et al. [1] in Fig. 3. The close correspondence between the present solutions and earlier findings demonstrates the validity, accuracy, and reliability of the proposed FEM approach.

Fig. 4 shows the effect of the axial compression load on the dmf (Fig. 4a) and the ndd at the mid-span (Fig. 4b) without the damping under three moving loads with d=L/4 in case of n=2 and Ω=0. It is shown that the dmf and the mid-span ndd of the FG beam increase as the axial compressive force increases, the stiffness of the beam decreases. The beam undergoes more oscillations when the velocity of the moving load is under 100 m/s. Moreover, the curves corresponding to P_e=5000kN, 10000kN are very close to the case without compressive load (Pe=0), it also proves that the compressive loads considered are very small compared with the critical load. In the following studies, the compressive load P_e=5000kN is selected to investigate the dmf and the ndd of the beam.

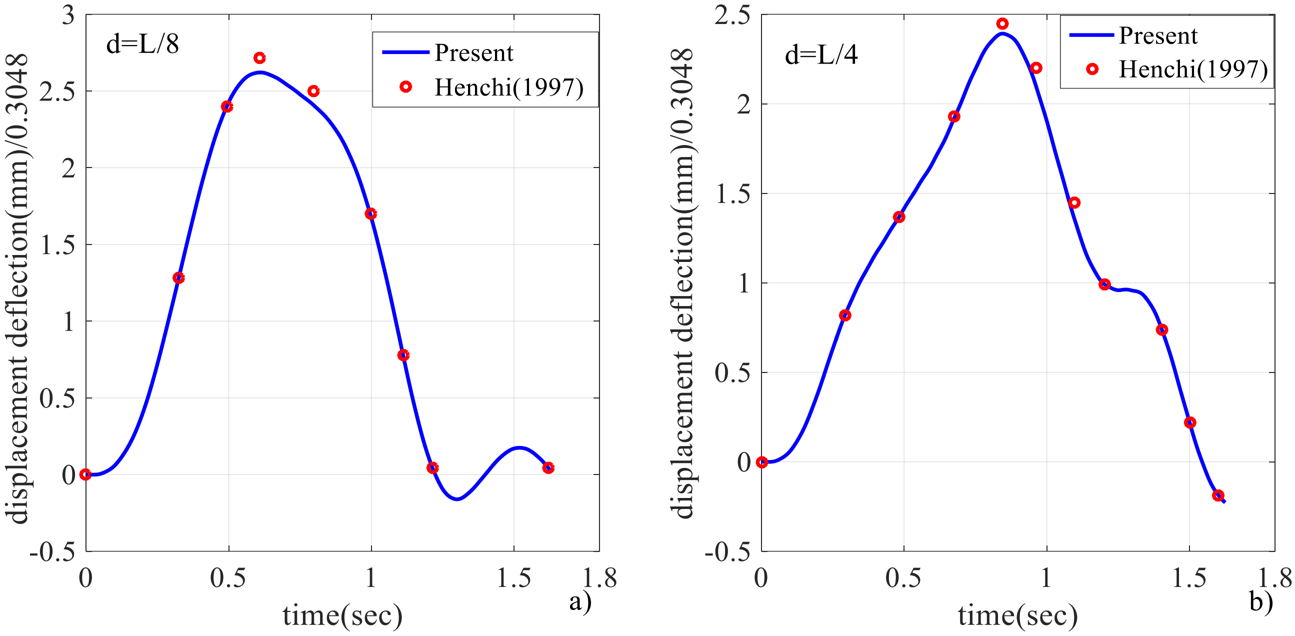

Fig. 3. Changes of the ndd for different values of the space between the three moving forces at v = 22.5m/s and P_e =0, Ω=0: a) d = L/8, b) d= L/4.

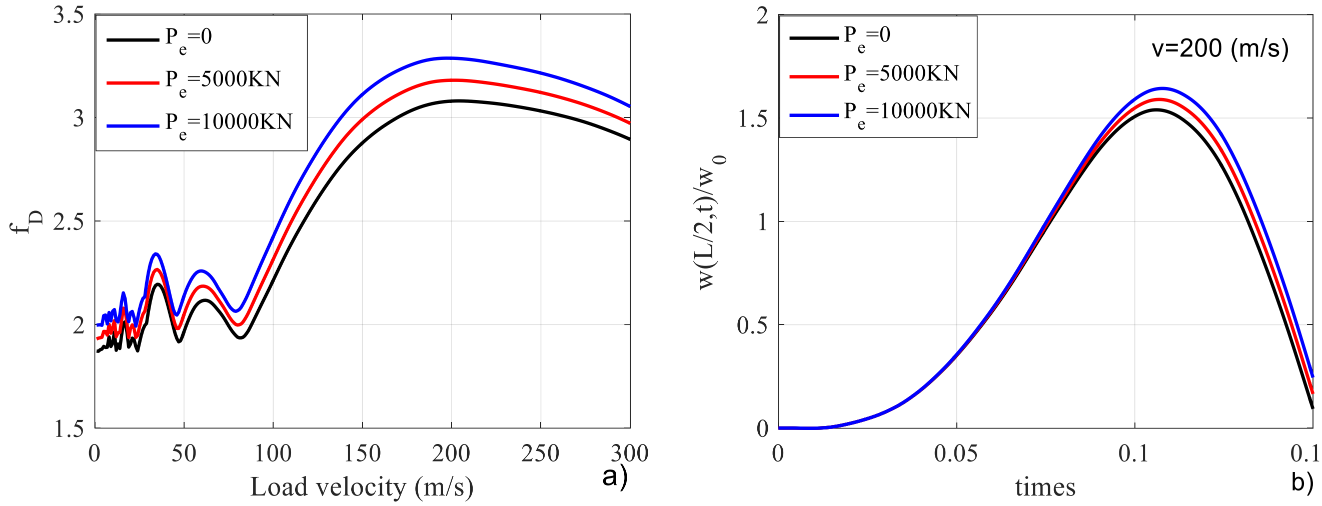

Fig. 4. The effect of the axial compression force on the dmf and the ndd without damping in case of n=2, Ω=0, and under three loads with d=L/4: a) The dmf; b) The ndd at v=200m/s.

Fig. 5 depicts the effect of the ς on the dmf (Fig. 5a) and the ndd (Fig. 5b) under an axial compression force P_e=5000kN and three moving loads traveling together with d=L/4 in case of n=2 and Ω=0. The results indicate that increasing the damping ratio leads to reductions in both the dmf and mid-span ndd, while also suppressing the oscillatory behavior of the dmf for all moving load velocities. When the damping ratio $\varsigma \leq 1.10^{-2}$, the dmf exhibits a maximum at a specific critical moving load velocity. Furthermore, an increase in the damping ratio leads to a reduction in both the maximum dmf and the corresponding critical moving load velocit. It is observed that for damping ratios above 5.10^{-2}, the dmf diminishes monotonically across all considered moving load velocities. In the following studies, the damping ratio $\varsigma=0.5.10^{-2}$ is selected to investigate the dmf and the ndd of the beam.

Figs. 6-7 show the influence of the excitation frequency and the velocity of moving loads on the dmf (Fig. 6a, Fig. 7a), the ndd (Fig. 6b, Fig. 7b) of the FG beam under an the axial compression force P_e=5000kN and multiple moving harmonic loads with d=L/4 in case of n=2 and ς=0.5.10^{-2}. It is noted that Ω=0 is responding to the constant moving loads and $\Omega \neq 0$ is responding to the harmonically varying moving loads. It is showed that the dmf and the mid-span ndd increase markedly as the excitation frequency varies from 20rad/s to 60rad/s. Specially, the dmf reaches the peak at Ω=40rad/s. This is explained by the fact that the excitation frequency Ω=40rad/s is nearly coincides with the natural frequency ω=39.83rad/s, and resonance phenomena occur for these parameters. These results demonstrate that the excitation frequency of the moving harmonic loads is a governing parameter in determining the dmf and ndd of the FG beam in such scenarios. Moreover, the beam undergoes more oscillations when the velocity of the moving forces is less than 100 m/s. It is observed that the dmf decreases progressively with increasing moving load velocity.

Fig. 8 depicts the effect of the number of moving loads with d=L/4 on the dmf when n=2, ς=0.5.10^{-2} and P_e=5000kN in case of Ω=0 (Fig. 8a) and Ω=40rad/s (Fig. 8b). It is observed that increasing the number of moving forces on the beam leads to higher maximum dmf values; however, these increases are not uniform with respect to the number of loads. Moreover, the dmf of FG beam under a moving harmonic load (Ω=40rad/s) is significantly higher than the dmf of a beam under a moving constant load (Ω=0), especially in the case of the velocity of moving harmonic loads is under 150m/s. This is due to the inertial force generated by forced vibration and the resonance effect when the excitation frequency is close to the natural frequency of the beam (ω=39.83rad/s).

Fig. 9 shows the effects of the distance between forces of three moving forces traveling together on the dmf with n=2, ς=0.5.10^{-2} and P_e=5000kN in case of Ω=0 (Fig. 9a) and Ω=40 rad/s (Fig. 9b). The results indicate that a larger distance between successive loads leads to a decrease in the peak dmf as well as in the number of oscillations of the ndd at the beam mid-span. This is due to when the spacing between the loads is small, their combined effect on the beam is greater than when the loads are spaced farther apart. Moreover, the dmf of FG beam under a moving harmonic force is significantly higher than the dmf of a beam under a moving constant load, especially in the case of the velocity of moving harmonic loads is under 150m/s.

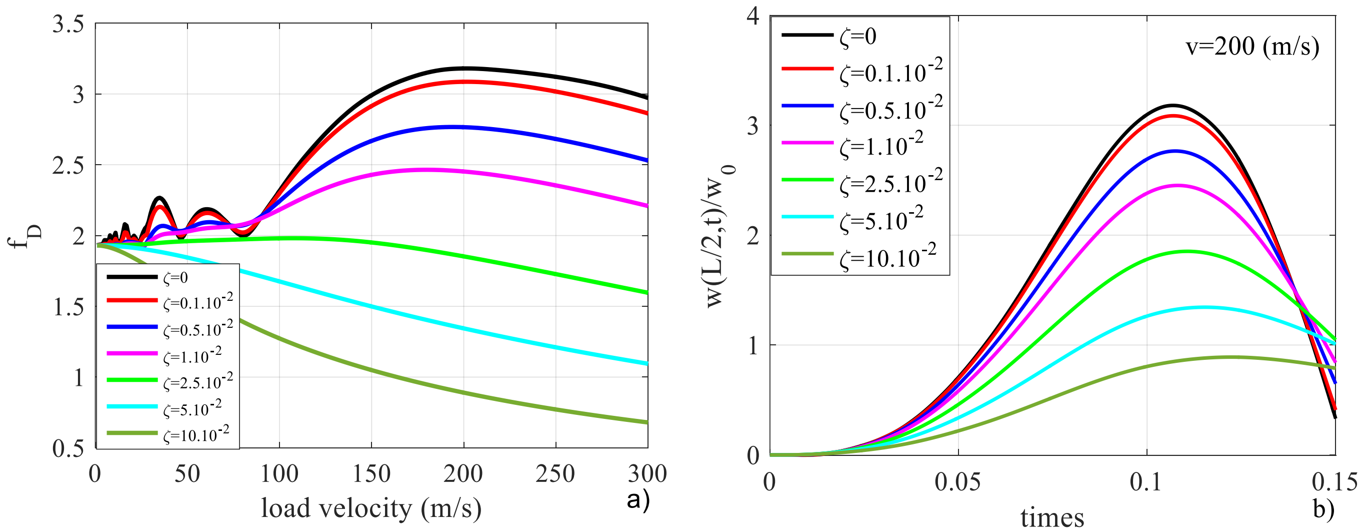

Fig. 5. The effect of the ς on the dmf and the ndd in case of n=2, Ω=0, P_e=5000kN, and under three loads with d=L/4: a) The dmf; b) The ndd at v=200m/s.

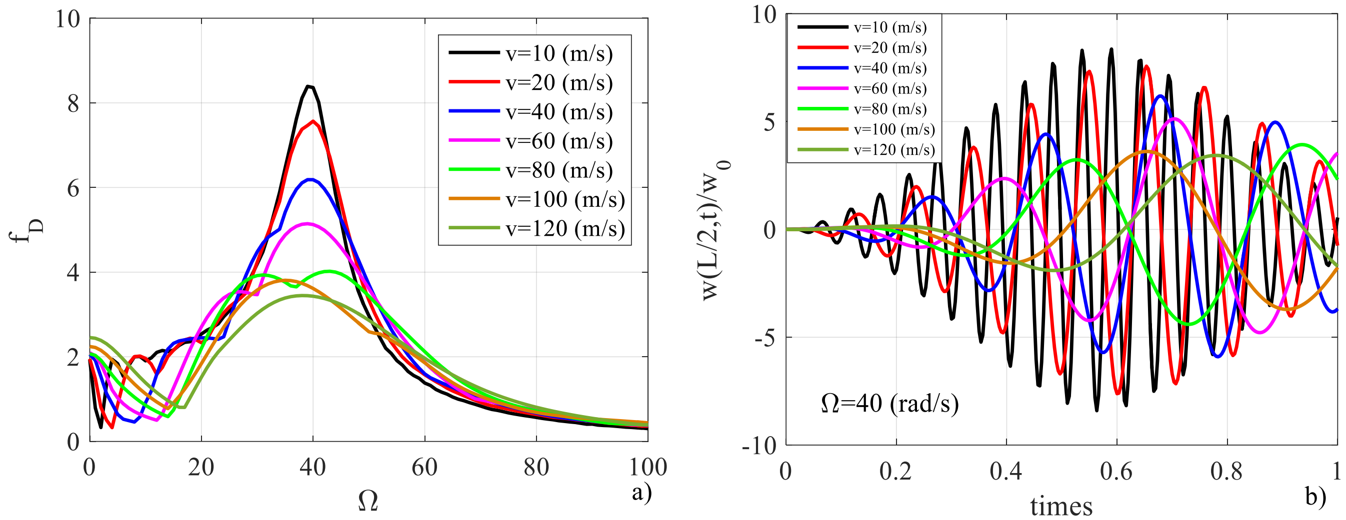

Fig. 6. The effect of the excitation frequency on the dmf and the ndd in case of n=2, ς=0.5.10^{-2}, P_e= 5000kN, and under three moving loads with d=L/4: a) The dmf; b) The ndd at v=20m/s

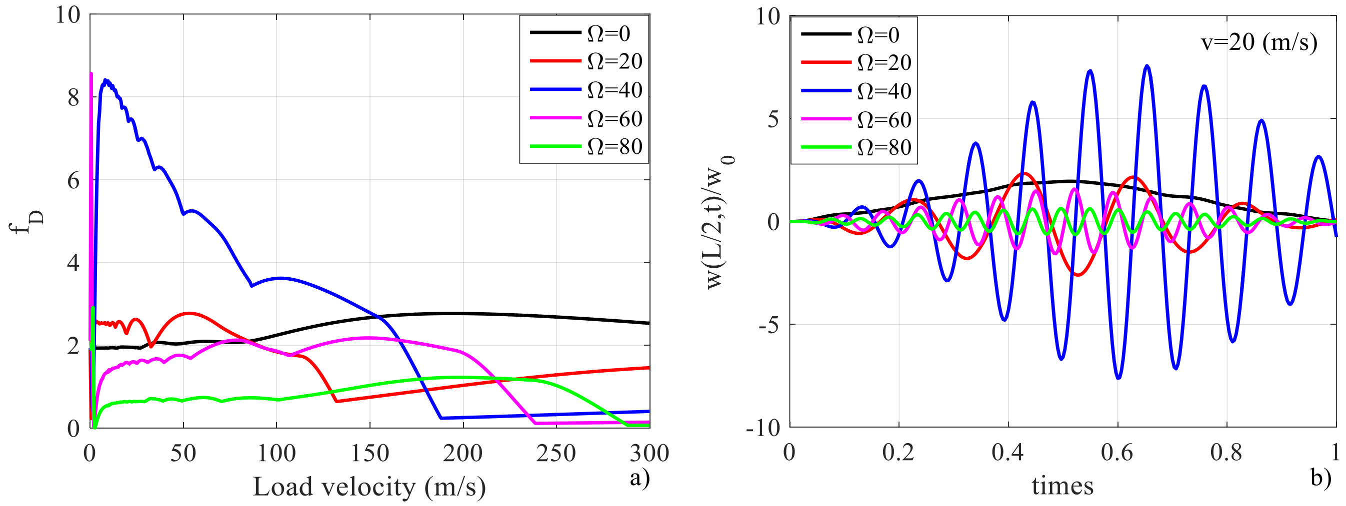

Fig. 7. The effect of the load velocity on the dmf and the ndd with n=2, ς=0.5.10^{-2}, P_e=5000kN and under three loads with d=L/4: a) The dmf; b) The ndd

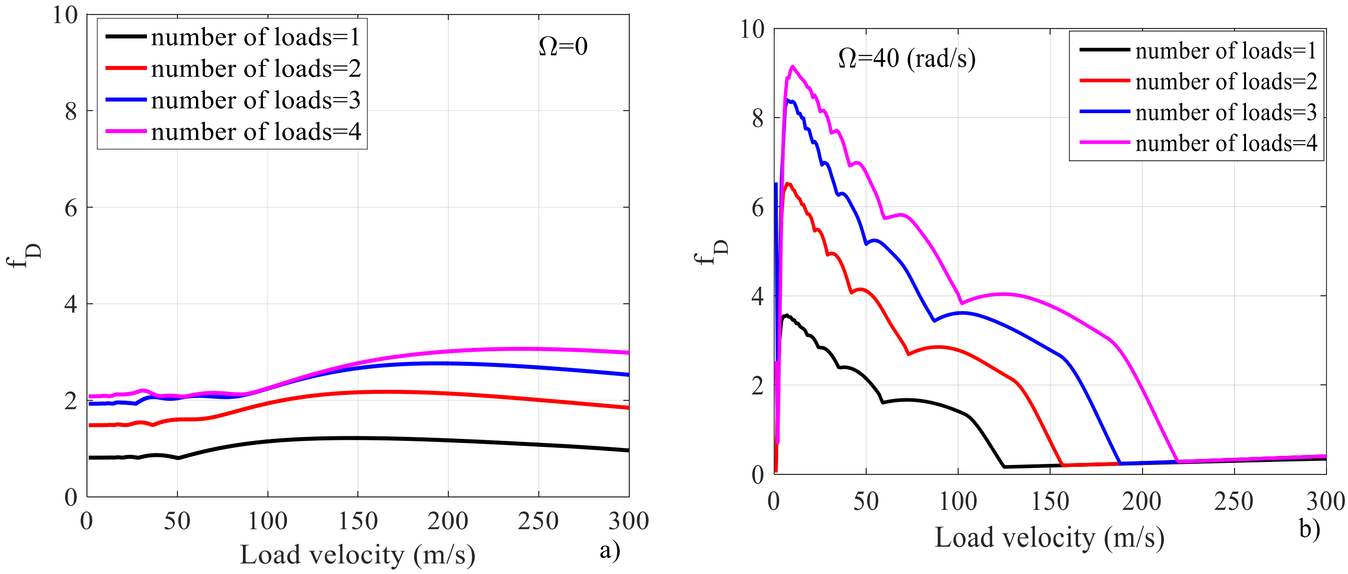

Fig. 8. The effect of the number of moving forces with d=L/4 on the DMF when n=2, ς=0.5.10^{-2} and P_e=5000kN: a) Ω=0; b) Ω=40rad/s

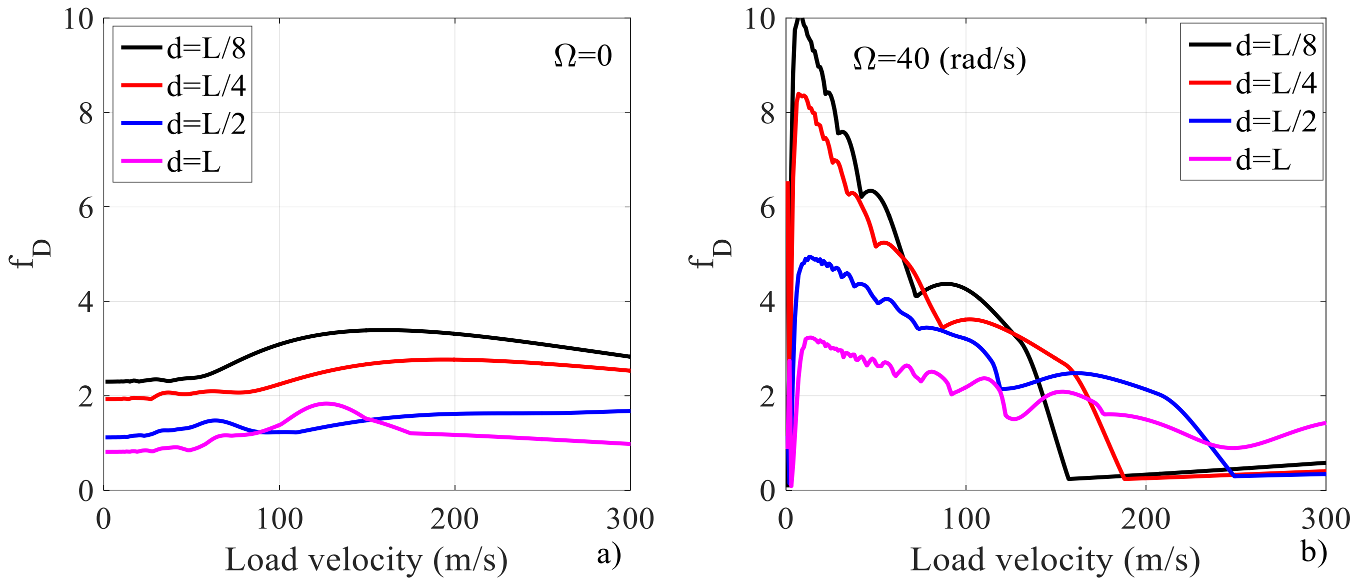

Fig. 9. The effect of the spacing between loads of multiple moving forces on the dmf with n=2, $\varsigma=0.5.10^{-2}$, P_e =5000kN: a) Ω=0; b) Ω=40rad/s

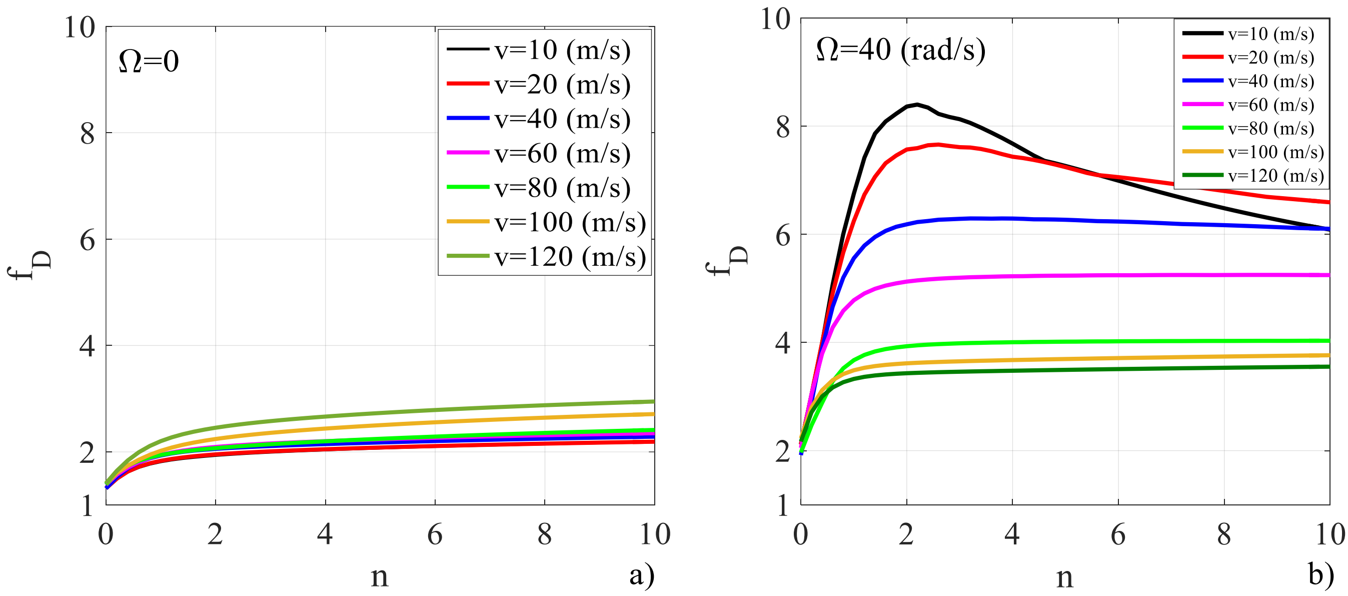

Fig. 10. The effect of the n on the dmf under three moving loads with d=L/4 when $\varsigma=0.5.10^{-2}$, P_e = 5000kN: a) Ω=0; b) Ω=40rad/s

Fig. 10 illustrates the effect of the volume fraction index n on the dmf under three moving loads with d=L/4 when $\varsigma=0.5.10^{-2}$, P_e = 5000kN in the case of Ω=0 (Fig. 10a) and Ω=40 rad/s (Fig. 10b). It is shown that increasing the volume fraction index and the load velocity, especially the load velocity is under 40m/s, lead to increase the dmf in two cases: a) a moving load without a harmonic oscillation form; b) a moving load with a harmonic oscillation form when $n \leq 2$. For constant loads, as the material parameter n increases, the system becomes stiffer, leading to an increase in the dmf as the velocity increases. Otherwise, increasing the volume fraction index and the load velocity lead to decrease the dmf when n > 2 and the load velocity is less than 40m/s for moving harmonic load. Moreover, the dmf of FG beam under a moving harmonic force is significantly higher than the dmf of a beam under a moving constant force, especially in the case of the load velocity is less than 60m/s.

Fig. 11 depicts the influence of elastic modulus ratio on the dmf under three moving force with d=L/4 when ς = 0.5.10^{-2}, P_e = 5000kN in the case of Ω=0 (Fig. 11a) and Ω=40 rad/s (Fig. 11b). It is shown that increasing the elastic modulus ratio and the load velocity, especially the load velocity is under 40m/s, lead to decrease the dmf in two cases: a) a moving load without a harmonic oscillation form; b) a moving load with a harmonic oscillation form when the elastic modulus ratio is greater than or equal to 1.75 ($E_2/E_1 \geq 1.75$). From the figures, it can be observed that for moving constant loads, the dmf decreases gradually as the elastic modulus ratio between the two layers increases. In contrast, for harmonically moving loads, the effect of the elastic modulus ratio is significant when the excitation frequency is close to resonance frequency and when the elastic moduli of the top and bottom layers are nearly equal. Otherwise, increasing the elastic modulus ratio and the load velocity lead to increase the dmf when the elastic modulus ratio is less than 1.75 ($E_2/E_1<1.75$) and the load velocity is less than 40m/s. Moreover, the dmf of FG beam subjected to a moving harmonic force is significantly higher than the dmf of a beam subjected to a moving constant load, especially in the case of the load velocity is less than 60m/s.

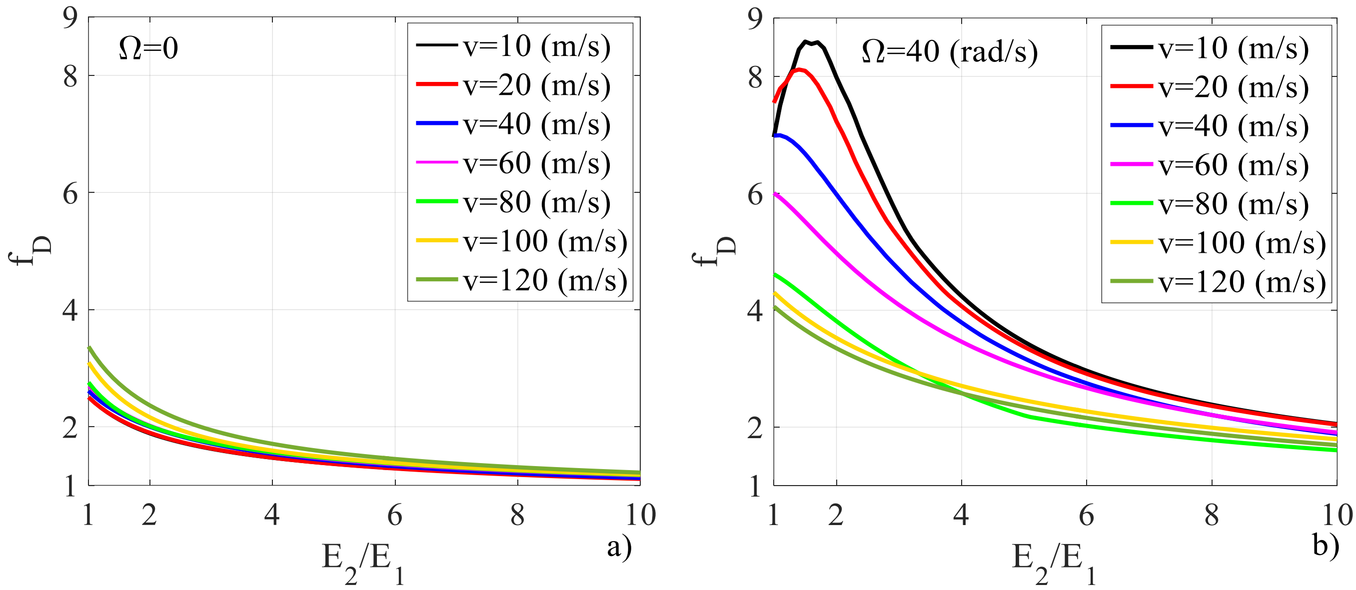

Fig. 11. The effect of the Young's modulus ratio on the dmf under three moving loads with d=L/4 when ς=0.5.10^{-2}, P_e=5000kN: a) Ω=0; b) Ω=40rad/s.

5. Conclusions

The dynamic response of the viscoelastic FG beam under axial compression and several moving forces has been examined. The Kelvin–Voigt model is used to account for damping in the dynamic analysis of the FG beams. The motion equations of the viscoelastic FG beams under axial compression and moving loads are derived via FEM. The present results agree well with published data. Based on the obtained results, the key conclusions of this investigation are presented as follows:

a) The axial compression force, damping ratio and frequency of the moving harmonic loads significantly influence the dmf and the mid-span ndd.

b) The dmf and the mid-span ndd of the viscoelastic FG beam increases in the cases:

+ The axial compression force increases;

+ The damping ratio is under 1.10^{-2};

+ The excitation frequency of moving harmonic loads is from 20rad/s to 60rad/s;

+ The number of moving force increase;

+ The spacing between successive loads in the moving load convoy is reduced.

+ The material parameter of the FG beam increases.

c) The study also highlights the role of the excitation frequency of the moving load, as well as its distinct influence, compared to moving loads with constant amplitude, on the DMF and dynamic response of FG beams. These effects significantly influence the vibration response of the viscoelastic FG beam.

The present formulation may be extended to investigate more complex structural configurations, including multiple-stepped and multi-span macro- and micro-beams subjected to various boundary conditions.

6. Scope and limitations of the study

The present formulation is established for viscoelastic functionally graded Timoshenko beams whose material properties vary along the thickness direction according to the Kelvin–Voigt viscoelastic model. The formulation may also be adapted for: (a) Euler–Bernoulli beam theory; (b) microbeams with two-dimensional material gradation; and (c) hysteretic damping models. Moreover, the proposed method can be applied to FG beams with varying taper ratios along the longitudinal direction by employing suitable finite element discretizations.

It should be noted, however, that the current study does not consider FG beams subjected to moving masses or moving vibration systems. In addition, thermo-mechanical coupling effects are beyond the scope of the present work.

Acknowledgements

This research is funded by University of Transport and Communications (UTC) under grant number T2026-CB-017TD.

Data availability

The authors declare that the data supporting the findings of this study are available within the paper.

Conflict of interests

The authors declared no potential conflicting/competing interests with respect to the research, authorship, and/or publication of this article.

Consent to participate

All authors participated in the research work reported in this paper.

Declaration of Generative AI

During the preparation of this work, the authors do not use Generative AI and AI-assisted technologies tools in order to generate the content of the manuscript.

References

[1]. K. Henchi, M. Fafard, G. Dhatt, M. Talbot. (1997). Dynamic behaviour of multi-span beams under moving loads. *Journal of Sound and Vibration*, 199(1), 33-50. https://doi.org/10.1006/jsvi.1996.0628

[2]. S.-M. Kim. (2004). Vibration and stability of axial loaded beams on elastic foundation under moving harmonic loads. *Engineering Structures*, 26(1), 95-105. https://doi.org/10.1016/j.engstruct.2003.09.001

[3]. T. Kocatürk, M. Şimşek. (2006). Vibration of viscoelastic beams subjected to an eccentric compressive force and a concentrated moving harmonic force. *Journal of Sound and Vibration*, 291(1-2), 302-322. https://doi.org/10.1016/j.jsv.2005.06.024

[4]. Y. Cai, L. Zhang, J. Zhang, X. Fan, X. Lv, H. Chen. (2025). Bending-torsional vibration response of modified Timoshenko thin-walled beams under moving harmonic loads. *Applied Mathematical Modelling*, 137, 115724. https://doi.org/10.1016/j.apm.2024.115724

[5]. M. Şimşek, T. Kocatürk. (2009). Free and forced vibration of a functionally graded beam subjected to a concentrated moving harmonic load. *Composite Structures*, 90(4), 465-473. https://doi.org/10.1016/j.compstruct.2009.04.024

[6]. M. Şimşek, T. Kocatürk, Ş.D. Akbaş. (2012). Dynamic behavior of an axially functionally graded beam under action of a moving

harmonic load. *Composite Structures*, 94(8), 2358-2364. https://doi.org/10.1016/j.compstruct.2012.03.020

[7]. M. Şimşek. (2010). Vibration analysis of a functionally graded beam under a moving mass by using different beam theories. *Composite Structures*, 92(4), 904-917. https://doi.org/10.1016/j.compstruct.2009.09.030

[8]. Y. Wang, D. Wu. (2016). Thermal effect on the dynamic response of axially functionally graded beam subjected to a moving harmonic load. *Acta Astronautica*, 127, 171-181. https://doi.org/10.1016/j.actaastro.2016.05.030

[9]. M. Şimşek, M. Al-Shujairi. (2017). Static, free and forced vibration of functionally graded (FG) sandwich beams excited by two successive moving harmonic loads. *Composites Part B: Engineering*, 108, 18-34. https://doi.org/10.1016/j.compositesb.2016.09.098

[10]. W. Songsuwan, M. Pimsarn, N. Wattanasakulpong. (2018). Dynamic responses of functionally graded sandwich beams resting on elastic foundation under harmonic moving loads. *International Journal of Structural Stability and Dynamics*, 18(09), 1850112. https://doi.org/10.1142/S0219455418501122

[11]. Ş.D. Akbaş. (2017). Forced vibration analysis of functionally graded nanobeams. *International Journal of Applied Mechanics*, 9(7), 1750100. https://doi.org/10.1142/S1758825117501009

[12]. H. Ding, Y.-Q. Tang, L.-Q. Chen. (2017). Frequencies of transverse vibration of an axially moving viscoelastic beam. *Journal of Vibration and Control*, 23(20), 3504-3514. DOI: 10.1177/1077546315600311

[13]. A. Mohseni, M. Shakouri. (2020). Natural frequency, damping and forced responses of sandwich plates with viscoelastic core and graphene nanoplatelets reinforced face sheets. *Journal of Vibration and Control*, 26(15-16), 1165-1177. https://doi.org/10.1177/1077546319893453

[14]. Ş.D. Akbaş, Y.A. Fageehi, A.E. Assie, M.A. Eltaher. (2022). Dynamic analysis of viscoelastic functionally graded porous thick beams under pulse load. *Engineering with Computers*, 38, 365-377. https://doi.org/10.1007/s00366-020-01070-3

[15]. K. Yee, U.M. Kankanamalage, M.H. Ghayesh, Y. Jiao, S. Hussain, M. Amabili. (2022). Coupled dynamics of axially functionally graded graphene nanoplatelets-reinforced viscoelastic shear deformable beams with material and geometric imperfections. *Engineering Analysis with Boundary Elements*, 136, 4-36. https://doi.org/10.1016/j.enganabound.2021.12.017

[16]. Y. Cui, T. Zeng, M. Fan, R. Wu, G. Xu, X. Wang. J. Zhao. (2024). Dynamic analysis of viscoelastic functionally graded porous beams using an improved Bernstein polynomials algorithm. *Chaos, Solitons & Fractals*, 189, 115698. https://doi.org/10.1016/j.chaos.2024.115698

[17]. C.W. de Silva. (2007). Vibration damping, control, and design. *CRC Press*. https://doi.org/10.1201/9781420053227

[18]. L.T. Ha, T.V. Lien. (2025). Effect of the damping model to dynamic responses of the cracked functionally graded microbeams on the elastic foundation subjected to moving load. *Journal of the Brazilian Society of Mechanical Sciences and Engineering*, 47, 312. https://doi.org/10.1007/s40430-025-05605-x

[19]. T.V. Lien, L.T. Ha. (2025). Dynamic analysis of functionally graded viscoelastic beams on the elastic foundation under multiple moving loads. *Vietnam Journal of Mechanics*, 47(1), 90-108. https://doi.org/10.15625/0866-7136/22165

[20]. J.B. Kosmatka. (1995). An improved two-node finite element for stability and natural frequencies of axial-loaded Timoshenko beams. *Computers & Structures*, 57(1), 141-149. https://doi.org/10.1016/0045-7949(94)00595-T

[21]. M. Geradin, D.J. Rixen. (2015). Mechanical Vibrations: Theory and Application to Structural Dynamics, 3rd Edition. *Wiley*.